Slow-Motional ESR Spectra for Vanadyl Complexes and Their Model Dependence

Robert F. Campbell[†] **and Jack H. Freed***

Baker Laboratory of Chemistry, Cornell University, Ithaca, New York 14853 (Received: February 21, 1980)

The slow-motional ESR analysis appropriate for vanadyl(IV) ions is developed with an accurate treatment of the nonsecular contributions. This results in good agreement between theory and experiments on $VO(acac_2(pm))$ in toluene with axially symmetric magnetic parameters over the whole motional range when a Brownian motion model is used. It is also found that a slightly modified motional narrowing theory based upon the stochastic Liouville equation leads to improved agreement between theory and experiment for $VO(acac)_2$ in toluene which also obeys a Brownian motion model. It is shown that vanadyl slow-tumbling spectra are very sensitive to model (even more so than nitroxides). In particular, experiments on $VO(H_2O)_5^{2+}$ in aqueous solution are approximately fit by a model of moderate jump, while those on $VO(NCS)_4^{2-}$ could only be crudely fit by temperature-dependent variations in model. The theory given here is appropriate for any $S = 1/2$ radical with a single nuclear spin I provided only the high-field approximation is valid, so that nonsecular terms may be treated by a perturbation approach. The effects of (1) angular-dependent transition probabilities and (2) field- vs. frequency-swept spectra upon the slow-motional theory are also discussed.

I. Introduction

The paramagnetic VO^{2+} ion is a well-known spin probe with many applications in ESR spectroscopy. Some more recent studies have pointed out the need for a rigorous slow-motional line-shape analysis in order to correctly elucidate the effects of the molecular dynamics.[1] Recently Bruno et al.[2] have developed an extension of the Freed, Bruno, and Polnaszek (FBP) slow-motional line-shape theory[3] based upon the stochastic Liouville equation (SLE) for the case of VO^{2+}. While in most respects the extension was straightforward, Bruno et al. realized the importance of explicit inclusion of nonsecular contributions at least to second-order perturbation theory, since the VO^{2+} magnetic parameters are about an order of magnitude greater than those of nitroxides for which the FBP theory was largely developed. The correction method of Bruno et al. was an extension of a van Vleck-type of perturbation scheme developed by Polnaszek, Bruno, and Freed.[4] While their extension is not the rigorous perturbation result, it has the property of reducing to the correct results in the motionally narrowed regime.

Though this work of Bruno et al. clearly demonstrated a rather good agreement between theory and experiment, their analysis failed to reproduce the details of the VO^{2+} slow-motional spectra as the motion slows beyond the incipient slow-motional region. They conjectured that this was due either to limitations of their perturbation analysis or to the fact that axially symmetric parameters were utilized in the theoretical analysis, although the experiments were on $VO(acac)_2$ with magnetic tensors that exhibit small deviations from axial symmetry.

Through a thorough analysis of the problem, we have found that these discrepancies are the result of an incomplete treatment of the nonsecular contributions to the spin Hamiltonian. Thus, in this paper we present a complete formulation for the calculation of VO^{2+} ESR line shapes in isotropic liquids and clearly demonstrate its quantitative validity by applying it to experimental spectra obtained from vanadyl complexes displaying axial (as well as slightly asymmetric) magnetic tensors.

As a consequence of these careful studies we also find that the VO^{2+} line shapes are very sensitive to deviations

[†] NIH Postdoctoral Fellow 1976–1978. FMC Corporation, Chemical Group, Box 8, Princeton, NJ 08540.

from Brownian rotational diffusion in the isotropic liquids we used. Bruno et al. were not able to observe such effects in their work with isotropic liquids,[5] presumably, in part, because the inaccuracies in spectral simulation were of the same order as model-dependent effects in the slow-motional region sensitive to such effects. In fact, our results show that slow-motional VO^{2+} spectra are *even more* sensitive to motional model than nitroxide spectra effects,[6] to the extent that models (viz. moderate jump vs. free diffusion), which could hardly be distinguished in the latter case,[6] are clearly distinguishable in the former case. This is perhaps the most interesting aspect of the present work, justifying the greater complexity of the analysis.

We also consider the importance of other effects on slow-tumbling spectra, for inorganic ions, which were not important for nitroxides (viz. anisotropy in the transition moment, the validity of a van Vleck perturbation scheme, and the effects of field-swept rather than frequency-swept experiments).

In section II, we present our theoretical analysis and the resulting set of coupled algebraic equations for the coefficients, C_{Km}^L, in the eigenfunction expansion of the density matrix from which the slow-tumbling spectrum is predicted. Also included in this section are the appropriate nonsecular contributions to these equations. These expressions are in a generalized form, and therefore applicable to any system of $S = 1/2$, I, described by coincident axially symmetric hyperfine and **g** tensors.

In section III, the SLE is rigorously tested by extensive comparisons of calculated spectra with those obtained from four experimental systems: $VO(acac_2(Pn))$ in toluene, $VO(H_2O)_5^{2+}$ in aqueous sucrose solution, $VO(NCS)_4^{2-}$ in ethyl acetate, and $VO(acac)_2$ in toluene. Analysis and discussion of these results are presented in section IV. The computer program is discussed in section V and conclusions appear in section VI. Discussion of other theoretical aspects appears in the Appendices.

II. Theory

The SLE method has been developed as a general approach to the calculation of EPR line shapes. In this section, we apply it to the vanadyl(IV) probe, in particular, and to spin $S = 1/2$ inorganic ions.

We start with the total spin Hamiltonian, $\mathcal{H}_s(\Omega)$, which

is separated in a form convenient for a perturbation-type treatment of the nonsecular contributions, so that

$$\mathcal{H}_s(\Omega) = \mathcal{H}_0 + \mathcal{H}_1^{(sec+pseudosec)}(\Omega) + \mathcal{H}_1^{(nonsec)}(\Omega) + \epsilon(t) \tag{1a}$$

Now, it is well established that (a) the vanadyl ion (a d^1 transition metal ion) is paramagnetic possessing a single unpaired electron; (b) in dilute solution the primary magnetic interactions contributing to the spin Hamiltonian are due to interaction of this single electron moment with both the external magnetic field (i.e., the electron Zeeman interaction) and the ^{51}V nuclear moment, $I = 7/2$ (i.e., the intramolecular electron–dipolar interaction); (c) the principal axes of the **g** and **A** tensors are coincident; and (d) the **g** and **A** tensors are nearly always axially symmetric. If we take advantage of this knowledge, as well as neglect the nuclear Zeeman[7] term, the spin Hamiltonian becomes

$$\mathcal{H}_0 = g_0(\beta_e/\hbar)B_0 S_z - 2bI_z S_z \tag{1b}$$

$$\mathcal{H}_1^{(sec+pseudosec)} = [F + D'I_z]\mathcal{D}_{0,0}^2(\Omega)S_z + [\mathcal{D}_{0,1}^2(\Omega)I_+ - \mathcal{D}_{0,-1}^2(\Omega)I_-]DS_z \tag{1c}$$

$$\mathcal{H}_1^{(nonsec)} = [b + (D'/4)\mathcal{D}_{0,0}^2(\Omega)][I_+S_- + I_-S_+] + [(3/8)^{1/2}F - DI_z][\mathcal{D}_{0,-1}^2(\Omega)S_- - \mathcal{D}_{0,1}^2(\Omega)S_+] - D[\mathcal{D}_{0,-2}^2(\Omega)I_-S_- + \mathcal{D}_{0,2}^2(\Omega)I_+S_+] \tag{1d}$$

$$\epsilon(t) = \tfrac{1}{2}\gamma_e B_1[S_+ e^{-i\omega t} + S_- e^{i\omega t}] \tag{1e}$$

where the following definitions apply:

$$b \equiv -|\gamma_e|A_0/2$$

$$F \equiv \tfrac{2}{3}(g_\| - g_\perp)(\beta_e/\hbar)B_0$$

$$D \equiv |\gamma_e|(A_\perp - A_\|)/(6)^{1/2}$$

$$D' \equiv -(8/3)^{1/2}D$$

$$g_0 \equiv \tfrac{1}{3}(g_\| + 2g_\perp)$$

$$A_0 \equiv \tfrac{1}{3}(A_\| + 2A_\perp)$$

The $\mathcal{D}_{0,m}^2(\Omega)$ are the orientation-dependent Wigner rotation matrices; $\hat{S}$ and $\hat{I}$ are the electron and nuclear spin operators, respectively; $g_\|$, $g_\perp$ and $A_\|$, $A_\perp$ (in gauss) are the principal values of the **g** and **A** tensors; g_0 and A_0 (in gauss) are the isotropic g value and isotropic A value, $|\gamma_e|$ is the magnitude of the electron magnetogyric ratio; β_e is

the Bohr magneton; and B_0 is the magnitude of the externally applied magnetic field.

Now, following the usual SLE formulation,[3] and using the generalized energy level scheme given in Figure 1, we obtain (in the absence of saturation and neglecting nonsecular contributions for the moment) eq 2a, a generating equation for the 64 coupled algebraic equations for the

$$\left[(\omega - \omega_0) + 2\left(m + \frac{n}{2}\right)b - i(T_2^{-1} + \tau_L^{-1})\right]\overline{C}_{0,n}^L \times$$
$$(2m + 2I + 2n + 2, 2m + 2I + 1; 2m + 2I + 2,$$
$$2m + 2I + 2n + 1) + (-1)^{n+1}\left[F + D'\left(m + \frac{n}{2}\right)\times\right.$$
$$\sum_{L'} N(L,L')\begin{pmatrix}L & 2 & L'\\ 0 & 0 & 0\end{pmatrix}\begin{pmatrix}L & 2 & L'\\ -n & 0 & n\end{pmatrix}\overline{C}_{0,n}^L(2m + 2I +$$
$$2n + 2, 2m + 2I + 1; 2m + 2I + 2, 2m + 2I + 2n +$$
$$1) + (-1)^{n+1}\Delta\left(\frac{D}{2}\right)\sum_{L'} N(L,L')\begin{pmatrix}L & 2 & L'\\ 0 & 0 & 0\end{pmatrix}\times$$
$$\begin{pmatrix}L & 2 & L'\\ -n & 1 & n-1\end{pmatrix}\left[f(J,-m)\overline{C}_{0,n-1}^{L'}(2m + 2I + 2n + 2,\right.$$
$$2m + 2I + 3; 2m + 2I + 4, 2m + 2I + 2n + 1) +$$
$$f(J,-m - n + 1)\overline{C}_{0,n-1}^{L'}(2m + 2I + 2n, 2m + 2I + 1;$$
$$\left.2m + 2I + 2, 2m + 2I + 2n - 1)\right] + (-1)^n \times$$
$$\Delta'\left(\frac{D}{2}\right)\sum_{L'} N(L,L')\begin{pmatrix}L & 2 & L'\\ 0 & 0 & 0\end{pmatrix}\begin{pmatrix}L & 2 & L'\\ -n & -1 & n+1\end{pmatrix}\times$$
$$\left[f(J,-m + 1)\overline{C}_{0,n+1}^{L'}(2m + 2I + 2n + 2, 2m + 2I - 1;\right.$$
$$2m + 2I, 2m + 2I + 2n + 1) + f(J,-m - n)\overline{C}_{0,n+1}^{L'}(2m +$$
$$2I + 2n + 4, 2m + 2I + 1; 2m + 2I + 2,$$
$$\left.2m + 2I + 2n + 3)\right] = \delta(L,0)\delta(n,0)(2)^{1/2} \tag{2a}$$

coefficients, C_{Km}^L, which determine the ESR spectrum of the vanadyl(IV) probe in isotropic liquids, where the absorption line shape, $P(\omega)$, is given by eq 2b. Previously

$$P(\omega) \propto \text{Im} \sum_{m=-I}^{I} C_{0,0}^0(2m + 2I + 2, 2m + 2I + 1) \tag{2b}$$

undefined variables are ω, the spectrometer microwave frequency; ω_0, the externally swept magnetic field in angular frequency units; I, the nuclear spin ($I = 7/2$ for vanadyl); T_2^{-1}, the orientation independent half-width at half-height in angular frequency units; τ_L^{-1} is the Lth eigenvalue of the isotropic rotational diffusion equation (τ_L^{-1} for the various rotational models have been given explicitly elsewhere),[6] and n is the "order" of the transition, where $n = 0, 1, 2, ..., 2I$ corresponding to allowed, singly forbidden, doubly forbidden, ..., $2I$-fold forbidden ESR transitions.[3] The quantity $\begin{pmatrix}L & 2 & L'\\ 0 & 0 & 0\end{pmatrix}$ is a $3j$ symbol, whose values are tabulated or given by formulas in standard references.[8] The coefficient $\overline{C}_{0,n}^L(a,b')$ is the matrix element $\langle a|C_{0,n}^L|b'\rangle$ and refers to the ESR transition $a \to b'$ (with the prime

General:
(Allowed transitions)

$|\tfrac{1}{2}, m\rangle$
$\overline{[2m+2I+1]}$

$m = I, I-1, \ldots\ldots, -I$

$|-\tfrac{1}{2}, m\rangle$
$\overline{[2m+2I+2]}$

Vanadyl (Allowed and Forbidden Transitions)
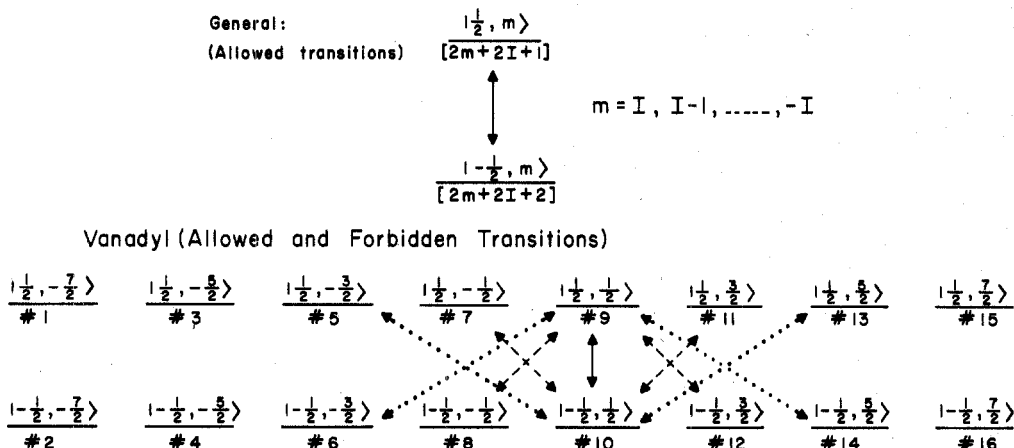
Figure 1. Generalized energy level and transition scheme. The notation is $|M_s, M_I = m\rangle$ for the energy levels, and these levels are numbered according to the bracketed terms (e.g., $[2m + 2I + 1]$ for $I = 1$ and $m = +1$ corresponds to state 5). Typical allowed transitions (—), singly forbidden transitions (---), doubly forbidden transitions (⋯).

referring to $M_s = -$ and unprime to $M_s = +$ and a and b refer, in general, to different nuclear spin configurations). Also

$$N(L,L') = [(2L + 1)(2L' + 1)]^{1/2} \qquad (2c)$$

$$f(J,-m) = [I(I + 1) - m(m + 1)]^{1/2} \qquad (2d)$$

$$\bar{C}^L_{0,n}(a,b';ba') = \frac{1}{(2)^{1/2}}[C^L_{0,n}(a,b') \pm C^L_{0,-n}(b,a')] \quad (2e)$$

$$\bar{C}^L_{0,0}(a,a';a,a') = (2)^{1/2}C^L_{0,0}(a,a') \qquad (2f)$$

where the plus sign is used for even n and the minus sign for odd n. Note that coefficients $\bar{C}^L_{0,n}$ where $n > L$ are by definition not allowed.

One uses eq 2a to obtain the 64 coupled coefficient equations of vanadyl(IV) as shown in Chart I.

The above result is applicable to any axially symmetric $S = 1/2$ probe with arbitrary I and, as such, is a straightforward generalization of PBF.[2,3]

Nonsecular Contributions. It is well known that, because vanadyl(IV) complexes have substantial intramolecular magnetic interactions, both the shift and line-width contributions originating from the nonsecular part of the spin Hamiltonian have significant effects on the EPR spectrum. Here, we present the complete perturbation treatment, and we take into account both shift and line-width contributions to the allowed and forbidden ESR transitions.

In the high-field approximation when $|\mathcal{H}_1^{\text{nonsec}}(\Omega)| \ll \omega_0$, it is possible to use a perturbation-type scheme for the complex symmetric matrices by application of a van Vleck transformation.[4] The complete form of this perturbation theory appropriate for vanadyl(IV) probes has the following term added to eq 2a:

$$\sum_{\substack{L'K'm' \\ L''K''m''}} \sum_{i,j,k} \langle LKm|\mathcal{H}_1^{\text{X,nonsec}}(\Omega)_{ij}|L''K''m''\rangle \times$$
$$\langle L''K''m''|\mathcal{H}_1^{\text{X,nonsec}}(\Omega)_{jk}|L'K'm'\rangle \bar{C}^{L'}_{K'm'}(k)V_{ijk}(L,L',L'') \quad (3)$$

where i and k are the usual transitions referred to in Figure 1, and j's are "eigenstate pair" transitions[9,10] (i.e., $\mathcal{H}_1^X(\Omega)_{ij}$ is the ijth matrix element of the superoperator $\mathcal{H}_1^X(\Omega)$). Now

$$V_{ijk}(L,L',L'') \equiv$$
$$\tfrac{1}{2}[(E_{i,LKm} - E_{j,L''K''m''})^{-1} + (E_{k,L'K'm'} - E_{j,L''K''m''})^{-1}] \quad (4)$$

where the dependence of V_{ijk} on K, m, etc. is implied but not explicitly shown, with

$$E_{i,LKm} \equiv \omega(i) + i\tau_{LKm}^{-1} \qquad (5)$$

where $\omega(i)$ is the resonance frequency of the ith transition (including, in general, the diagonal contribution from the secular and pseudosecular terms in $\mathcal{H}_1(\Omega)$), with the real part of $E_{i,LKm}$ giving the nonsecular shift contribution and the imaginary part giving the nonsecular line-width contribution. We note that since $\omega(j) \approx 0$ for the case of eigenstate pair transitions, j, eq 5 can be approximated as

$$E_{j,LKm} \approx i\tau_{LKm}^{-1} \qquad (5')$$

Further, in the high-field approximation (i.e., $\omega(i) \sim \omega(k) \sim \omega$) eq 4 becomes

$$V_{ijk}(L,L',L'') =$$
$$\tfrac{1}{2}[(\omega_0 + i(\tau_L^{-1} - \tau_{L''}^{-1}))^{-1} + (\omega_0 + i(\tau_{L'}^{-1} - \tau_{L''}^{-1}))^{-1}] \quad (4')$$

The final result for the nonsecular contributions written

Chart I

for $n = 0$, $m = I, I - 1$, $\ldots, -I$		8 "allowed transitions"
for $n = 1$, $m = I - 1$, $I - 2, \ldots, -I$		7 "singly forbidden transitions"
$\vdots$	$\vdots$	
for $n = 7$, $m = -I$		multiply forbidden transitions

$\Delta = 1$, $\Delta' = 1$ for $n > 0$
$\Delta = 0$, $\Delta' = 2$ for $n = 0$

further $\displaystyle\sum_{L'}$ is restricted
to $L' = L, L \pm 2$

in the generalized scheme of eq 2a requires that the complex expression, eq 6 (given in Appendix A), be added to the left-hand side of eq 2a.

It is the more complete form of eq 4' that represents the primary correction to the work of Bruno et al.,[2,5] and it has a very different rotational model dependence compared to their simplified expression.[11] [Also nonsecular contributions to all forbidden transitions are given.]

The effects of (1) angular-dependent transition probabilities, (2) field-swept instead of frequency-swept ESR spectra, and (3) the van Vleck transformation used are discussed in Appendix B, while the implications for motionally narrowed line widths are discussed in Appendix C.

III. Results

In order to rigorously test our line-shape formulation, based upon axially symmetric magnetic interactions, we made extensive comparisons with spectra obtained from four experimental systems: $VO(acac_2(pn))$ in toluene, $VO(H_2O)_5^{2+}$ in aqueous sucrose solution, $VO(NCS)_4^{2-}$ in ethyl acetate, and $VO(acac)_2$ in toluene. The first three were chosen because they gave rigid-limit spectra unambiguously characterized by axially symmetric magnetic interactions, while $VO(acac)_2$ was employed to test the applicability of such axial simulations to a system displaying small asymmetric magnetic interactions.[2] The results of this study show that (a) the formulation, as verified by $VO(acac_2(pn))$, is sound for axially symmetric systems over the entire motional scale (i.e., motionally narrowed to the rigid limit), (b) the $VO(H_2O)_5^{2+}$ and $VO(NCS)_4^{2-}$ systems display non-Brownian rotational diffusion behavior, and (c) the formulation is applicable to slightly asymmetric systems such as $VO(acac)_2$ for $\tau_R \lesssim 3 \times 10^{-9}$ s (i.e., valid in the slow tumbling region).

(A) Determination of Magnetic Tensor Components. All magnetic tensor components (i.e., $A_\parallel$, $A_\perp$, $g_\parallel$, $g_\perp$) were obtained from the 77 K frozen solution EPR spectrum via computer simulation. The simulation was based upon the usual axial rigid-limit program for computing the spectrum as a superposition of Lorentzian line shapes.[11] Magnetic parameters obtained are given in Table I.

In order to investigate the possibility of any temperature dependence of the magnetic parameters, the trace of the magnetic tensors (**A** and **g**) was compared with the isotropic magnetic parameters determined from the room temperature spectrum. One sees that only in the case of $VO(H_2O)_5^{2+}$ does there appear to be a slight temperature dependence to the magnetic parameters (i.e., here TR[**A**] $\neq A_0$).

(B) $VO(acac_2(pn))$ in Toluene. Experimental and respective simulated spectra over a range of temperatures are shown in Figure 2. They illustrate the changes oc-

TABLE I: Magnetic Parameters for Vanadyl Complexes

complex	$A_{\parallel}$ ($\pm 0.5\%$), G	$A_{\perp}$ ($\pm 0.08\%$), G	A_0 ($\pm 0.5\%$),[a] G	A_0^{calcd} ($\pm 0.7\%$),[b] G	$g_{\parallel}$ (± 0.002)	$g_{\perp}$ (± 0.001)	g_0^a (± 0.002)	$g_0^{calcd\ c}$ (± 0.002)
VO(acac$_2$(pm))	-179.8	-62.5	-101.7	-101.6	1.956	1.983	1.977	1.974
VO(NCS)$_4^{2-}$	-180.0	-64.0	-102.6	-102.7	1.946	1.980	1.971	1.969
VO(H$_2$O)$_5^{2+}$	-201.4	-75.5	-115.7	-117.5	1.933	1.976	1.964	1.962
VO(acac)$_2$	-191.0	-68.7^d	-109.0	-109.5	1.945	1.981^e	1.971	1.969

[a] From room temperature isotropic liquid solution. [b] $A_0^{calcd} \equiv \frac{1}{3}(A_{\parallel} + 2A_{\perp})$. [c] $g_0^{calcd} \equiv \frac{1}{3}(g_{\parallel} + 2g_{\perp})$. [d] $A_x = -69.6$, $A_y = -67.8$, and $A_{\perp} = \frac{1}{2}(A_x + A_y)$. [e] $g_x = 1.979$, $g_y = 1.985$, and $g_{\perp} = \frac{1}{2}(g_x + g_y)$.
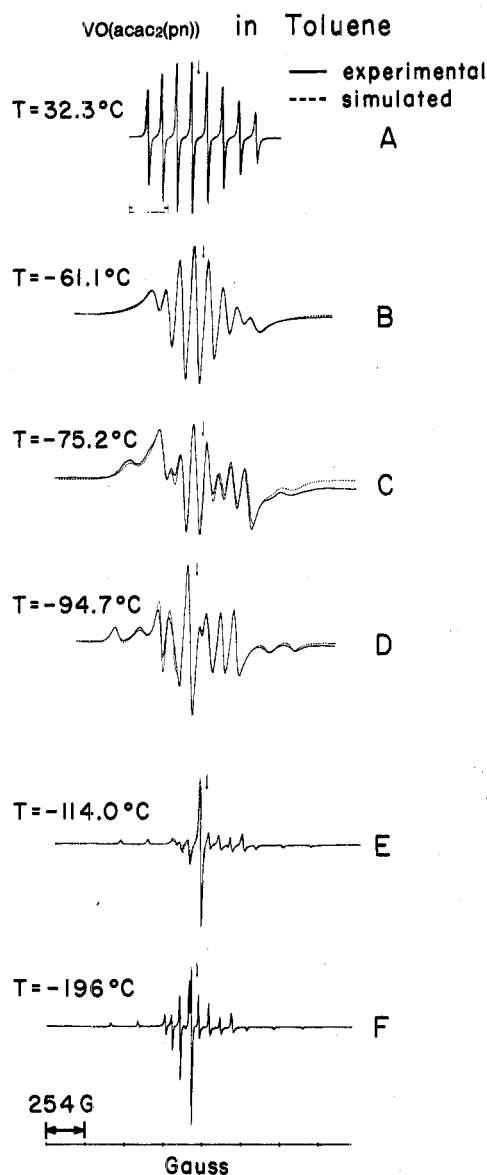
Figure 2. Comparison of experimental and simulated spectra from the rapid motional to the rigid limit for VO(acac$_2$(pn)) in toluene. All simulations use a Brownian rotational diffusion model with τ_R^B defining the rotational correlation time. α'' is the residual line-width contribution. (A) $\tau_R^B = 2.06 \times 10^{-11}$ s, $\alpha'' = 1.7$ G; (B) 2.63×10^{-10} s, 1.7 G; (C) 5.00×10^{-10} s, 1.7 G; (D) 2.25×10^{-10} s, 1.7 G; (E) 5.0×10^{-8} s, $\alpha'' = 6$ G; (F) rigid limit.

curring in line shape from the motionally narrowed region to the rigid limit. The simulated spectra are given by the dashed lines and were calculated by using eq 2a, 2b, and 6 with the Brownian rotational diffusion model (non-Brownian models gave poor agreement). All spectra were calculated by varying τ_R and T_2^{-1}, using the rigid limit parameters listed in Table I. As one can see, the fit over the entire range of spectra is quite good even in the slow-tumbling region. These results clearly show that previous

difficulties[2] were the result of incomplete treatment of the nonsecular contributions via the van Vleck perturbation-type scheme.

Spectrum 2A shows the motionally narrowed spectrum obtained at $T = 32.3$ °C. Such spectra are characterized by Lorentzian line shapes and occur when $\mathcal{H}_1(\Omega)\tau_R \ll 1$. The calculated spectrum was obtained with $\tau_R = 2.1 \times 10^{-10}$ s and $T_2^{-1} = 1.6$ G. For such simulations, as well as those extending into the slow tumbling region, there was a weak dependence of the observed relative intensities of the resonance lines on T_2^{-1}. Thus variation of both τ_R and T_2^{-1} is necessary to obtain the best spectral fit.

Spectrum 2B ($T = -61.1$ °C) is representative of the so-called "incipient slow-tumbling" region which is characterized by asymmetric absorption line shapes that are shifted relative to their motionally narrowed positions. Such spectra occur when $\mathcal{H}_1(\Omega)\tau_R \sim 1$. Here $\tau_R = 2.6 \times 10^{-10}$ s and $T_2^{-1} = 1.7$ G.

As the rotational correlation time becomes longer (i.e., $\mathcal{H}_1(\Omega)\tau_R > 1$), the slow-tumbling spectra 2C ($T = -75.2$ °C) and 2D ($T = -94.7$ °C) are obtained. The best fits are obtained for $\tau_R = 5.0 \times 10^{-10}$ s, $T_2^{-1} = 1.7$ G and $\tau_R = 2.3 \times 10^{-9}$ s, $T_2^{-1} = 1.7$ G, respectively. Molecular tumbling such that the anisotropy in the magnetic interactions is clearly evident characterize such spectra. Although perfect agreement between experiment and simulation is not obtained, the overall spectral fit is still very good and clearly shows that the problems in fitting the central portion of slow-tumbling spectra have been resolved. [Some problems in fitting the outer extrema were associated with experimental problems in base-line variation occurring over large field sweeps.]

The great similarity between spectrum 2E and that of the rigid limit, spectrum 2F, identifies it to be of the so-called "near rigid-limit" type. The simulation yielded $\tau_R = 5.0 \times 10^{-8}$ s, $T_2^{-1} = 6$ G.

(C) VO(H$_2$O)$_5^{2+}$ *in Aqueous Sucrose Solution (pH 2.0)*. Experimental spectra as a function of temperature compared with respective simulation, based upon a model of moderate jump diffusion[6] using the magnetic parameters in Table I, are shown in Figure 3A. Additionally, each moderate jump diffusion simulation is compared with free and Brownian diffusion models in Figure 3B. Note that the predictions of free and jump diffusion are clearly distinguishable, although this was not the case for nitroxides (where $I = 1$).

Although the spectral fits based upon the moderate jump diffusion model (weak jump gave poor results while there was negligible change between moderate ($R\tau = 2$) and strong jumps ($R\tau \rightarrow \infty$)) cannot be considered excellent (the spectral fit becoming poorer with increasing τ_R), it is clear from Figure 3 that jump diffusion gives the best overall agreement to experiment.

(D) VO(NCS)$_4^{2-}$ *in Ethyl Acetate*. Experimental and simulated spectra for this system are shown in Figure 4. Attempts to simulate the experimental spectra, for the different temperatures, gave poor spectral fits with any of the usual diffusion models: Brownian, free, or jump dif-
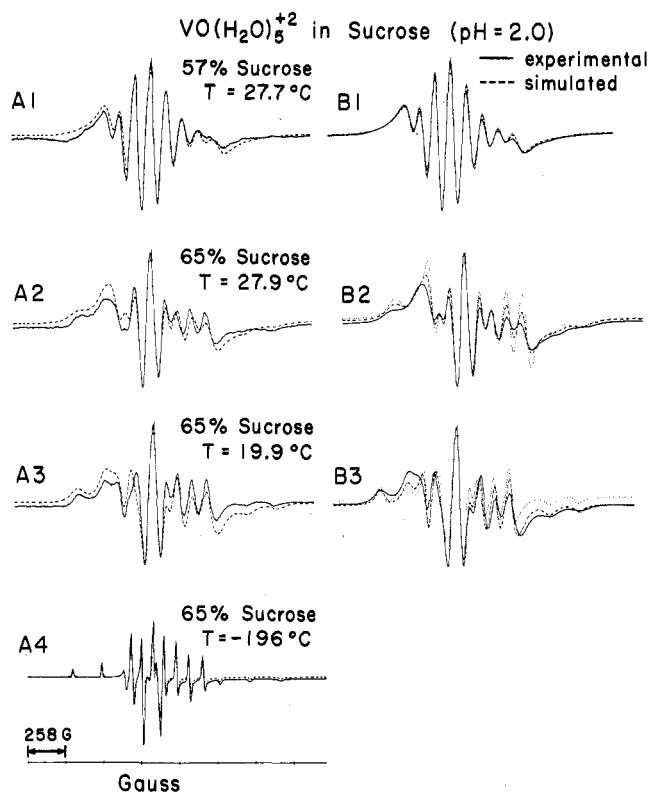
Figure 3. Model dependence of $VO(H_2O)_5^{2+}$ in sucrose. (Series A) Comparison of experiment with moderate jump diffusion. (Series B) Comparison of moderate jump diffusion (solid lines) with its free (dashed lines) and Brownian (dotted lines) diffusion equivalent. [$R\tau = 2$ (i.e., moderate jump)[6] gave best agreement in all cases.] (A1) $\tau_R^J = 3.4 \times 10^{-10}$ s, $\alpha'' = 2.0$ G; (A2) 6.0×10^{-10} s, 2.0 G; (A3) 9.0×10^{-10} s, 2.0 G; (A4) rigid limit. (B1) $\tau_R^J = 3.4 \times 10^{-10}$ s, $\tau_R^F = 3.0 \times 10^{-10}$ s, $\tau_R^B = 2.8 \times 10^{-10}$ s, $\alpha'' = 2.0$ G; (B2) 6.0×10^{-10} s, $\alpha'' = 2.0$ G for all cases; (B3) 9.0×10^{-10} s, 1.5×10^{-9} s, 3.0×10^{-9} s, respectively, $\alpha'' = 2.0$ G.

fusion. Although we were able to obtain a good spectral fit in the model-insensitive motionally narrowed region (not shown), the incipient and slow-tumbling regions yielded neither good nor model-consistent results. Thus, for the incipient slow-tumbling region (Figure 4A), the poor but closest fit was obtained with moderate jump diffusion, while for the slow-tumbling spectrum (Figure 4B), free diffusion gave the closest fit. In contrast the slower-tumbling spectrum (Figure 4C) was quite well described by Brownian diffusion.

(E) $VO(acac)_2$ in Toluene. Experimental and simulated spectra are shown in Figure 5. As stated earlier, this system was chosen to test the applicability of our formulation to a system described by asymmetric magnetic tensors. (The asymmetry is clearly seen in the rigid limit powder pattern, Figure 5C.) This system was found to be well described by Brownian rotational diffusion as indicated in parts A and B of Figure 5 where we show typical incipient and slow-tumbling spectrum. For the slow-motional spectrum best agreement was obtained with $A_\perp = A_x = 70.5$ G. Therefore these parameters were used to simulate the incipient slow-motional and rigid-limit spectra as well.

IV. Discussion

The dependence of τ_R vs. η/T is shown in Figure 6 for $VO(acac_2(pn))$. The good linear dependence over several orders of magnitude variation in τ_R is expected for a radical probe coupled strongly to the viscous modes of the solvent.[6,12] It may also be taken as further confirmation of the validity of the Brownian motional model.[6,12] We also
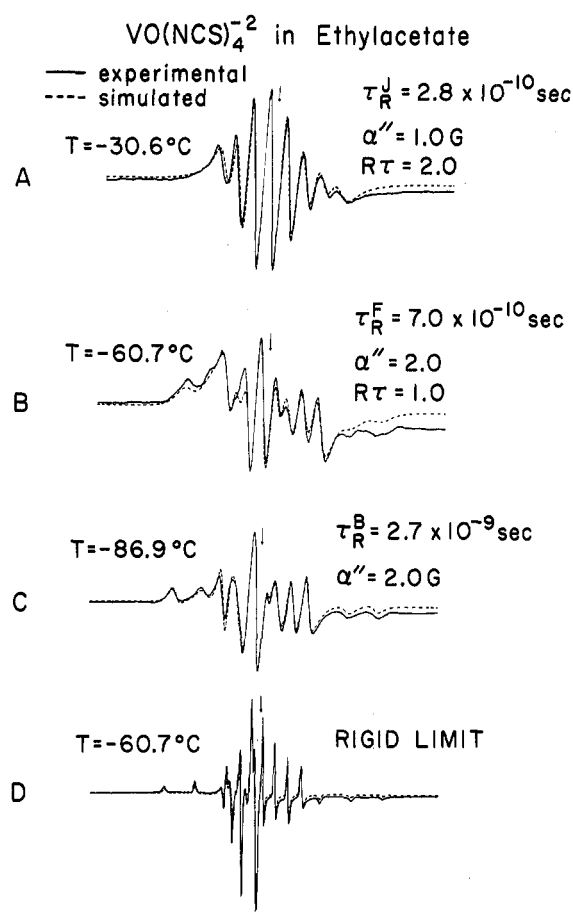
Figure 4. Model dependence of $VO(NCS)_4^{2-}$ in ethyl acetate. Note that A is approximately fit with moderate jump, B with free diffusion, and C with Brownian diffusion.

show a similar plot for $VO(acac)_2$ with our more limited data for that system. Since the molecular radius of $VO(acac)_2$ ($r_e \approx 3.4$ Å)[13] is slightly smaller than that of $VO(acac_2(pn))$ the values of τ_R are slightly larger. The structures of the vanadyl complexes appear in Figure 7. The validity of a Brownian rotational model for these large complexes (i.e., substantially larger than the molecules of solvent, viz. toluene) is no surprise.[13] The smaller nitroxide probes peroxylamine disulfonate ($r_e \approx 1.5$ Å in frozen water and in glycerol)[6,12] and PD-Tempone ($r_e \approx 2.4$ Å also in toluene)[12] were better fit by a moderate jump model.

Given the simplicity of the predicted results for ESR line shapes, one would not expect particularly unusual spin-relaxation behavior for these vanadyl complexes. Nevertheless, Hoel and Kivelson[14] in a study of vanadyl complexes in the motional narrowing region were particularly troubled by the residual line width, i.e., that which is not accounted for by Brownian rotational modulation of **A** and **g**. Since the magnetic tensor components are axially symmetric, the τ_R measured by ESR is really $\tau_\perp$, the rotational diffusion time about the axes perpendicular to the symmetry axis. Hoel and Kivelson[14] then suggest that perhaps the motion of the "disklike" vanadyl complexes about the symmetry axis, as measured by $\tau_\parallel$, is nonviscous but highly inertial; i.e., there is a substantial amount of "slip". This could lead to an anomalous increase in the spin-rotational relaxation time τ^{SR} with an anomalous increase in line width as the temperature decreases. They note that such a model might "explain" the residual line widths they observe in the lower temperature range of the motional narrowing region.

Such a model is in fact inconsistent with the more
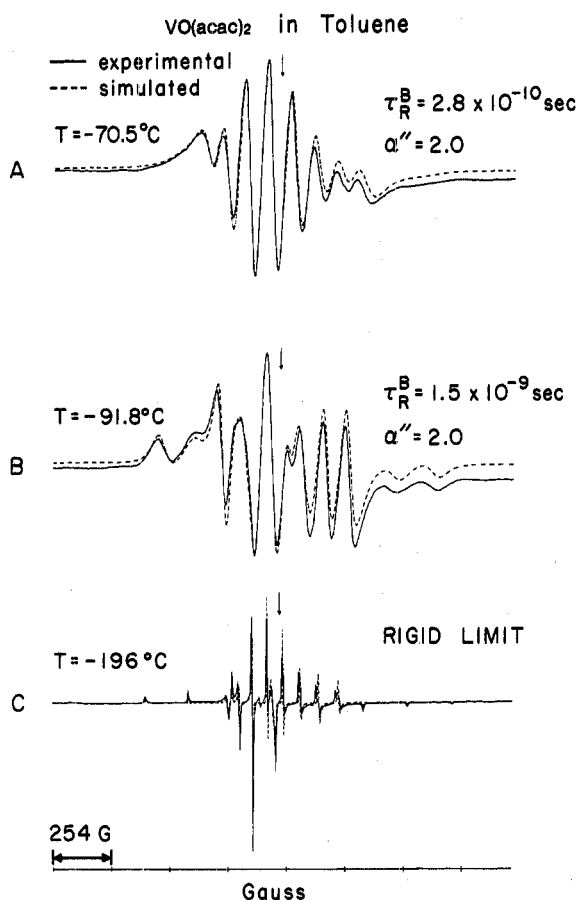
Figure 5. Comparison of experimental and simulated spectra for VO(acac)$_2$ in toluene. All simulations are with a Brownian rotational diffusion model.

Figure 6. $\tau_R(B)$ vs. η/T for VO(acac$_2$(pn)) in toluene and VO(acac)$_2$ in toluene.

Figure 7. Structures of the vanadyl complexes.

complete experimental results on the smaller PD-Tempone (in which effects of both $\tau_\parallel$ and $\tau_\perp$ are directly measured) as we have previously pointed out.[12,15] The results (on PD-Tempone) are consistent with both $\tau_\parallel$ and $\tau_\perp$ being dominated by the viscous modes, and actual T_1 measurements show no anomalous increase in spin-rotational relaxation but rather a steady decrease with reduced T.

Given our accurate analysis of VO(acac$_2$(pn)) and VO-(acac)$_2$ in the slow motional region, we can now examine these residual line widths over the whole motional region to the rigid limit. We show in Figure 8 the combined results of Wilson and Kivelson[16] on the residual line widths obtained in the motional narrowing region and our results from the slow-tumbling region. We see that a residual line width of about 1.7 G does not appear anomalous but rather constant from the incipient slow-motional region over orders of magnitude change in $\tau_\perp$ and η/T, to practically the rigid limit. This observation is inconsistent with a model proposing an increasing spin-rotational contribution as the temperature decreases. In fact, a "constant" residual line width of this order is typical of vanadyl complexes[1] and also of the nitroxide probes,[6,12,15] where it is largely associated with inhomogeneous broadening due to the contribution of unresolved superhyperfine structure from the ligand or intramolecular protons (or deuterons). The actual rigid-limit residual widths would further include inhomogeneous broadening due to solvent protons and to other small variations in local site. We thus conclude from our study that there is no evidence for substantial inertial effects in the rotational motion of these vanadyl complexes in toluene solvent. Our results for the other vanadyl complexes in more H-bonding solvents are consistent with these above comments (see below); it was in H-bonding
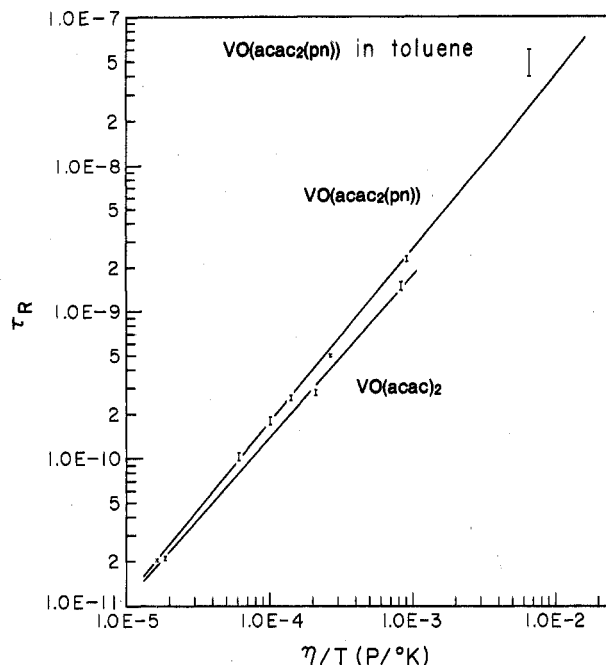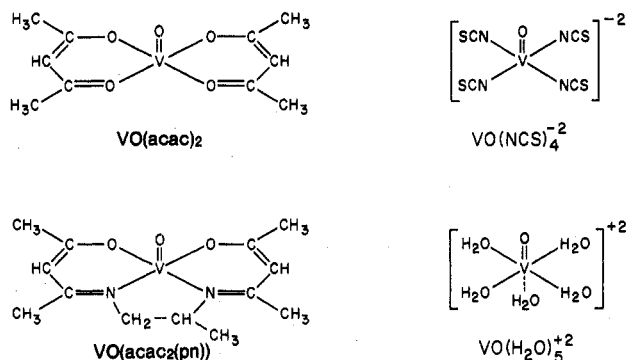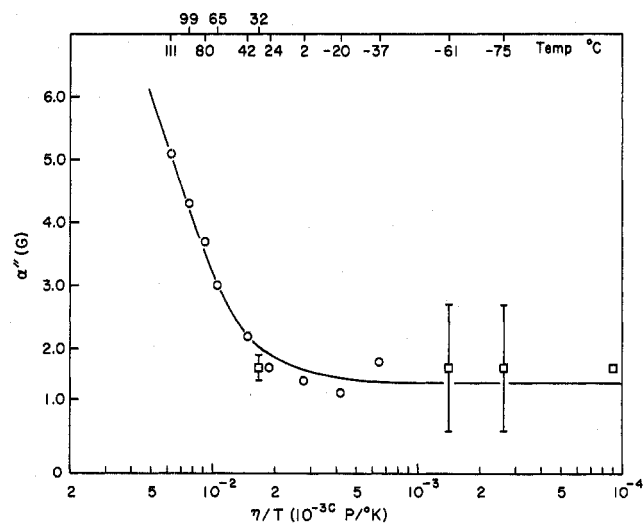
Figure 8. The residual line width (α'', i.e., T_2^{-1}) plotted vs. η/T. The motional narrowing values represented by the circles are from ref 16 and are for VO(acac)$_2$ in toluene; the squares are mostly from slow-motional simulations for VO(acac$_2$(pn)) in toluene.

alcoholic solvents that Hoel and Kivelson found the greatest discrepancies.

Our results for the $VO(H_2O)_5^{2+}$ system clearly display model dependence. We can further check the approximate fit to a moderate jump model by extrapolating the results for τ_R vs. η/T from the motion-narrowing region into the slow-motional region and comparing this extrapolated curve with the best τ_R values obtained for the different models.[6,12] This is done in Figure 9, and it demonstrates a preference for the moderate jump diffusional model. This result is not very conclusive in itself, because of some uncertainty in η (i.e., η was not measured directly but rather extrapolated from tables, cf. section V). [Note, however, that a residual line width of about 2 G is typical for our slow-tumbling fits.]

The fact that $VO(H_2O)_5^{2+}$ shows significant deviation from Brownian motion in its slow-tumbling ESR spectra is perhaps not surprising in view of its smaller size $r \approx 2.3$ Å (cf. Figure 7). The fact that it was not possible to obtain as good spectral fits as those obtained for the nitroxide probes PADS and PD-Tempone,[6,12] which also exhibit moderate jump diffusion, may be attributed to (i) the greater sensitivity of vanadyl spectra to motional model (as already noted), so that our simple modeling might be inadequate, and/or (ii) the possible role of solvent-induced "collisions" as water molecules exchange between the inner and outer hydration spheres.

The peculiar model dependence of $VO(NCS)_4^{2-}$ in ethyl acetate is perhaps more surprising, since the overall size is not much different from $VO(acac)_2$ and $VO(acac_2(pn))$ (cf. Figure 7) although there is a "spokelike" arrangement of the monodentate ligands, possibly allowing for more solvent penetration. It would be interesting to study such effects for a range of solvents.

V. Experimental Section

Sucrose Solutions (pH 2.0). Sucrose solutions of varying viscosities were prepared by weighing an appropriate amount of reagent grade sucrose and dissolving it in 0.010 m HCl. [The appropriate amount of sucrose for a given viscosity was obtained from published viscosity data.[17]] The resulting solutions were stored under $N_2(g)$ for 2 weeks in order to ensure both oxygen outgassing and complete dissolution of the sucrose.

Preparation of Vanadyl Complexes. (1) $VO(acac)_2$. Bis(acetylacetone)oxyvanadium(IV) was prepared by twice recrystallizing the reagent grade chemical, purchased from Alpha Products, from a saturated solution of spectroscopic grade acetone at 100 °C. The bright blue-green crystals were washed with dry ether and stored under vacuum in a desiccated bell jar.

(2) $VO(acac_2(pn))$. Bis(acetylacetone propylenediimine)oxyvanadium(IV) was prepared by the ligand-exchange reaction[18] between bis(acetylacetone)oxyvanadium(IV) and bis(acetylacetone)propylenediamine. The latter compound was prepared by the method of McCarthy et al.[19] The resulting gray-green product was recrystallized four times from boiling toluene which had been cooled to 0 °C. The final product was light gray-blue in color with a melting point of 200 ± 1 °C. It was then stored under vacuum in a desiccated bell jar.

(3) $VO(NCS)_4^{2-}$. Tetrakis(thiocyanato)oxyvanadium(IV) was prepared after the method of Hazell.[20] The product was redissolved in ethyl acetate and precipitated by the addition of anhydrous toluene so as to ensure an anhydrous product. Without this step, the ESR spectrum of the product consisted of a superposition of two spectra: one due to the tetrakis(thiocyanato) complex and the other due to a mixed complex of water and thiocyanate.

$$
+ [D^2] \Big[[(m+n-1)] \begin{pmatrix} L & 2 & L'' \\ n & -2 & -n+2 \end{pmatrix}\begin{pmatrix} L'' & 2 & L' \\ n-2 & 1 & -n+1 \end{pmatrix} - (m+n) \begin{pmatrix} L & 2 & L'' \\ -n & 0 & n \end{pmatrix}\begin{pmatrix} L'' & 2 & L' \\ -n+1 & 0 & -n+1 \end{pmatrix} \Big] \Big]
$$

$$
\times (f(J, -m-n+1) \bar{C}^{L'}_{o,n-1} {}^{(2m+2l+2n, 2m+2l+2l+1; 2m+2l+2, 2m+2l+2n-1)}
$$

$$
+ \Delta \Big((-1)^n N(L,L') \begin{pmatrix} L & 2 & L' \\ o & o & o \end{pmatrix}\begin{pmatrix} L & 2 & L' \\ n & -1 & -n+1 \end{pmatrix} \Big) \{ [(3/8)^{\frac{1}{2}} bF_o] [V(L,L',L) + V(L,L',L')] + [-bD] \big[[(m+1)V(L,L',L) + (m)V(L,L',L') \big] \} \}
$$

$$
+ V(L,L',L'',L'') N(L,L'') N(L'',L') \begin{pmatrix} L & 2 & L'' \\ o & o & o \end{pmatrix}\begin{pmatrix} L'' & 2 & L' \\ o & o & o \end{pmatrix} \{ [-(3/8)^{\frac{1}{2}} F_o D] \big[\begin{pmatrix} L & 2 & L'' \\ n & -2 & -n+2 \end{pmatrix}\begin{pmatrix} L'' & 2 & L' \\ n-2 & 1 & -n+1 \end{pmatrix} - \begin{pmatrix} L & 2 & L'' \\ -n & -1 & n+1 \end{pmatrix}\begin{pmatrix} L'' & 2 & L' \\ -n-1 & 2 & n-1 \end{pmatrix} \big] + [(3/8)^{\frac{1}{2}} F_o(D'/4)] \big[\begin{pmatrix} L & 2 & L'' \\ -n & o & n \end{pmatrix}\begin{pmatrix} L'' & 2 & L' \\ -n & 1 & n-1 \end{pmatrix} - \begin{pmatrix} L & 2 & L'' \\ n & -1 & -n+1 \end{pmatrix}\begin{pmatrix} L'' & 2 & L' \\ n-1 & o & -n+1 \end{pmatrix} \big]
$$

$$
+ [D^2] \Big[[(m+1)] \begin{pmatrix} L & 2 & L'' \\ n & -2 & -n+2 \end{pmatrix}\begin{pmatrix} L'' & 2 & L' \\ n-2 & 1 & -n+1 \end{pmatrix} - (m) \begin{pmatrix} L & 2 & L'' \\ -n & o & n \end{pmatrix}\begin{pmatrix} L'' & 2 & L' \\ -n & 1 & n-1 \end{pmatrix} \big] + [-D(D'/4)] \big[[(m+1)] \begin{pmatrix} L & 2 & L'' \\ -n & o & n \end{pmatrix}\begin{pmatrix} L'' & 2 & L' \\ -n & 1 & n-1 \end{pmatrix} - (m) \begin{pmatrix} L & 2 & L'' \\ n & -1 & -n+1 \end{pmatrix}\begin{pmatrix} L'' & 2 & L' \\ n-1 & o & -n+1 \end{pmatrix} \big] \Big] \}
$$

$$
\times (f(J, -m) \bar{C}^{L'}_{o,n-1} {}^{(2m+2l+2n+2, 2m+2l+2l+3; 2m+2l+4, 2m+2l+2n-1)}
$$

$$
+ \Delta' \Big((-1)^n N(L,L') \begin{pmatrix} L & 2 & L' \\ o & o & o \end{pmatrix}\begin{pmatrix} L & 2 & L' \\ n & 1 & -n-1 \end{pmatrix} \Big) \{ [-(3/8)^{\frac{1}{2}} bF_o] \big[V(L,L',L) + V(L,L',L') \big] + [bD] \big[[(m+n+1)V(L,L',L) + (m+n)V(L,L',L') \big] \} \}
$$

$$
+ V(L,L',L'') N(L,L'') N(L'',L') \begin{pmatrix} L & 2 & L'' \\ o & o & o \end{pmatrix}\begin{pmatrix} L'' & 2 & L' \\ o & o & o \end{pmatrix} \{ [(3/8)^{\frac{1}{2}} F_o D] \big[\begin{pmatrix} L & 2 & L'' \\ -n & -2 & n+2 \end{pmatrix}\begin{pmatrix} L'' & 2 & L' \\ -n-2 & 1 & n+1 \end{pmatrix} - \begin{pmatrix} L & 2 & L'' \\ n & -1 & -n+1 \end{pmatrix}\begin{pmatrix} L'' & 2 & L' \\ n-1 & 2 & -n-1 \end{pmatrix} \big] + [-(3/8)^{\frac{1}{2}} F_o(D'/4)] \big[\begin{pmatrix} L & 2 & L'' \\ n & o & -n \end{pmatrix}\begin{pmatrix} L'' & 2 & L' \\ n & 1 & -n-1 \end{pmatrix} - \begin{pmatrix} L & 2 & L'' \\ -n & -1 & n+1 \end{pmatrix}\begin{pmatrix} L'' & 2 & L' \\ -n-1 & o & n+1 \end{pmatrix} \big]
$$

$$
+ [-D^2] \Big[[(m+n+1)] \begin{pmatrix} L & 2 & L'' \\ -n & -2 & n+2 \end{pmatrix}\begin{pmatrix} L'' & 2 & L' \\ n-1 & 2 & -n-1 \end{pmatrix} - (m+n) \begin{pmatrix} L & 2 & L'' \\ n & o & -n \end{pmatrix}\begin{pmatrix} L'' & 2 & L' \\ -n & 1 & n-1 \end{pmatrix} \big] + [D(D'/4)] \big[[(m+n+1)] \begin{pmatrix} L & 2 & L'' \\ n & o & -n \end{pmatrix}\begin{pmatrix} L'' & 2 & L' \\ n & 1 & -n-1 \end{pmatrix} - (m+n) \begin{pmatrix} L & 2 & L'' \\ -n & -1 & n+1 \end{pmatrix}\begin{pmatrix} L'' & 2 & L' \\ -n-1 & o & n+1 \end{pmatrix} \big] \Big] \}
$$

$$
\times (f(J, -m-n) \bar{C}^{L'}_{o,n+1} {}^{(2m+2l+2n+4, 2m+2l+2n+1; 2m+2l+2, 2m+2l+2n+3)}
$$

$$
+ \Delta' \Big((-1)^n N(L,L') \begin{pmatrix} L & 2 & L' \\ o & o & o \end{pmatrix}\begin{pmatrix} L & 2 & L' \\ n & 1 & -n-1 \end{pmatrix} \Big) \{ [-(3/8)^{\frac{1}{2}} bF_o] \big[V(L,L',L) + V(L,L',L') \big] + [bD] \big[[(m-1)V(L,L',L) + (m)V(L,L',L') \big] \} \}
$$

$$
+ V(L,L',L'') N(L,L'') N(L'',L') \begin{pmatrix} L & 2 & L'' \\ o & o & o \end{pmatrix}\begin{pmatrix} L'' & 2 & L' \\ o & o & o \end{pmatrix} \{ [(3/8)^{\frac{1}{2}} F_o D] \big[\begin{pmatrix} L & 2 & L'' \\ -n & -2 & n+2 \end{pmatrix}\begin{pmatrix} L'' & 2 & L' \\ -n-2 & 1 & n+1 \end{pmatrix} - \begin{pmatrix} L & 2 & L'' \\ n & -1 & -n+1 \end{pmatrix}\begin{pmatrix} L'' & 2 & L' \\ n-1 & 2 & -n-1 \end{pmatrix} \big] + [-(3/8)^{\frac{1}{2}} F_o(D'/4)] \big[\begin{pmatrix} L & 2 & L'' \\ n & o & -n \end{pmatrix}\begin{pmatrix} L'' & 2 & L' \\ n & 1 & -n-1 \end{pmatrix} - \begin{pmatrix} L & 2 & L'' \\ -n & -1 & n+1 \end{pmatrix}\begin{pmatrix} L'' & 2 & L' \\ -n-1 & o & n+1 \end{pmatrix} \big]
$$

$$
+ [-D^2] \Big[[(m-1)] \begin{pmatrix} L & 2 & L'' \\ -n & -2 & n+2 \end{pmatrix}\begin{pmatrix} L'' & 2 & L' \\ n-1 & 2 & -n-1 \end{pmatrix} - (m) \begin{pmatrix} L & 2 & L'' \\ n & o & -n \end{pmatrix}\begin{pmatrix} L'' & 2 & L' \\ n & 1 & -n-1 \end{pmatrix} \big] + [D(D'/4)] \big[(m-1) \begin{pmatrix} L & 2 & L'' \\ n & o & -n \end{pmatrix}\begin{pmatrix} L'' & 2 & L' \\ n & 1 & -n-1 \end{pmatrix} - (m) \begin{pmatrix} L & 2 & L'' \\ -n & -1 & n+1 \end{pmatrix}\begin{pmatrix} L'' & 2 & L' \\ -n-1 & o & n+1 \end{pmatrix} \big] \Big] \}
$$

$$
\times (f(J, -m+1) \bar{C}^{L'}_{o,n+1} {}^{(2m+2l+2n+2, 2m+2l+2l-1; 2m+2l, 2m+2l+2n+1)}
$$

where: $\Delta = 1, \Delta' = 1$ for $n > o$

$\Delta = 0, \Delta' = 2$ for $n = o$

(6)

Figure 9. Comparison of τ_R vs. η/T for the different rotational diffusion models with the extrapolation of the motionally narrowed data: (---) motionally narrowed data and extrapolation.

Preparation of Vanadyl Solutions. (1) VO(acac)$_2$ and VO(acac$_2$(pn)) in toluene were prepared with spectroscopic grade toluene by standard vacuum line techniques. That is, toluene was first distilled over a sodium mirror and then distilled into a cold finger containing an appropriate amount of vanadyl complex. Solutions were then thoroughly outgassed by the repetitive freeze–thaw method. Resulting vanadyl concentrations were $\leq 8 \times 10^{-4}$ M and were low enough that intermolecular effects were negligible.

(2) VO(NCS)$_4^{2-}$ in ethyl acetate was prepared with reagent grade ethyl acetate prepared by the standard vacuum techniques described above.

(3) VO(H$_2$O)$_5^{2+}$ (i.e., penta(aquo)oxyvanadium(IV)) was prepared by dissolving reagent grade vanadyl sulfate, from Alpha Products, in 0.01 m H$_2$SO$_4$ which had been prepared from doubly distilled water. The resulting stock solution was 1.00 m as determined by standard spectrophotometric technique.

(4) VO(H$_2$O)$_5^{2+}$ in sucrose at pH 2.0 was prepared by mixing appropriate amounts of the 1.00 m VO(H$_2$O)$_5^{2+}$ stock solution with sucrose solution of the desired viscosity. The mixing and storage of these solutions was done under a positive pressure of N$_2$(g). [pH 2.0 was used because no appreciable oxidation of the vanadyl ion occurs at or below this pH.]

Viscosity Determinations. (1) Viscosities of sucrose solutions were determined from published tables.[17]

(2) Viscosities of toluene solutions as a function of temperature were determined from viscosity formulas for toluene.[21]

ESR Spectrometer. ESR spectra were recorded at X band with a Varian E-12 spectrometer with 100-kHz field modulation at a low enough modulation amplitude that no line-shape distortion was observed. Microwave power was always adjusted so that no saturation occurred. Temperature was controlled by a Varian E-257 variable-temperature unit and measured with a very fine gauge copper–constantan thermocouple placed along side the sample tube and extending to the center of the cavity. The temperature gradient over the ESR cavity (i.e., top to bottom of the active area) was ≤ 0.5 °C.

Field calibrations were obtained by the standard proton probe method. Normal sweep ranges were 2000 G.

Aqueous sucrose samples were recorded by using a Varian E-238 aqueous cavity and flat cell in order to obtain maximum sensitivity.

TABLE II: Computational Data

spectrum type	typical τ_R (B), s	typical L,n	typical computation time, s
motionally narrowed	2.0×10^{-11}	2,2	6
incipient slow motional	2.0×10^{-10}	6,2	12
slow motional	5.0×10^{-10}	8,2	22
slow motional	2.3×10^{-10}	12,3	78
near rigid limit	5.0×10^{-8}	24,7	4980

VI. Computer Program

Computation of ESR spectra via the stochastic Liouville method has been discussed elsewhere.[22] Therefore, only additions or refinements to this general format will be treated. First, since the coefficient equations (eq 2) are written in a generalized form, only minor changes involving I and m_I need to be made in order to convert the program to any $S = 1/2$, I system dominated by $\mathbf{g}$ and $\mathbf{A}$ interactions. Second, nonsecular contributions can be completely truncated so as to allow computational efficiency for systems possessing small intramolecular magnetic interactions. Third, in all but near-rigid-limit simulations inclusion of all forbidden transitions (i.e., $n = 1, ..., 7$) is not necessary in order to obtain spectral convergence. Therefore, n truncation was included in order to maximize computational efficiency for the faster motional spectra. Typical computation times (for an IBM 370/168 computer), as well as typical L and n values required for convergence,[23] may be found in Table II for various types of vanadyl spectra. (In general, non-Brownian diffusion models require longer L and n values.) Fourth, an option for the "approximate field swept" (see Appendix C) spectral computation has been included.

VII. Conclusion

We have shown that an accurate treatment of the nonsecular terms in the stochastic-Liouville formulation leads to very good agreement between theory and experiment for the axially symmetric vanadyl complex VO(acac$_2$(pn)) over the whole motional region when a Brownian motion model is used. The complexes VO(H$_2$O)$_5^{2+}$ and VO-(NCS)$_4^{2-}$ show significant deviations from simple Brownian diffusion and they exemplify the fact that vanadyl slow-tumbling spectra are very sensitive to motional model, because of (1) the many hyperfine lines which are affected to different extents by the motion and probably also because of (2) the sensitivity of the nonsecular correction terms to motional model. Thus more extensive studies with a range of vanadyl complexes and solvents would be worthwhile.

Appendix A

Here we present eq 6, which is the correction to be added to eq 2a. Because of coupling between such coefficients as $C_{0,0}^L(a,a')$ and the $C_{0,1}^{L'}(a,b')$, $C_{0,-1}^{L'}(b',a)$ the following approximation (valid within the spirit of a perturbation-type scheme) has been made so as not to introduce new coef-

ficients into the line-shape calculation as well as to preserve the validity of eq 2e:

$$[1/(2)^{1/2}][\epsilon_{0,1}^{L'}(a,b')C_{0,1}^{L'}(a,b') - \epsilon_{0,-1}^{L'}(b,a')C_{0,-1}^{L'}(b,a')] \rightarrow$$

$$\left(\frac{\epsilon_{0,1}^{L'}(a,b') + \epsilon_{0,-1}^{L'}(b,a')}{2}\right)\bar{C}_{0,1}^{L'}(a,b';b,a') \quad (6a)$$

In eq 6a $\epsilon_{0,1}^{L'}(a,b')$, etc. are the coefficients of the $C_{0,1}^{L'}(a,b')$, etc. Also we note that the $\sum_{L''}$ is restricted to $L'' = L, L \pm 2$ and $\sum_{L'}$ is restricted to $L' = L'', L'' \pm 2$. In the spirit of this perturbation-type scheme, we have neglected any coupling greater than $L' = L, L \pm 2$. [For *ordered* fluids this last approximation breaks down, cf. ref 5.]

Equation 6 is more complex than the result of Bruno et al.[2] (e.g., products of four $3-j$ symbols appear in eq 6 while in the simplified form of Bruno et al.[2,5] only products of two $3-j$ symbols appear), as required for a rigorous application of eq 3 with eq 4' and 5'.

Appendix B. Further Aspects of the Slow-Tumbling Theory

(1) Effects of Angular-Dependent Transition Probabilities on Slow-Motional Spectra. The usual slow-motional theories assume a nearly isotropic $\bar{g}$ tensor, so the ESR transition probabilities are very nearly orientation independent. However, for transition-metal ions, the $\bar{g}$ tensor is more anisotropic.

We consider here the corrections required for the slow-motional theory in this case. We consider the case of unsaturated line shapes for which we may write for the imaginary part of the rf magnetic susceptibility as[24,25]

$$\chi''_{xx}(\omega) = \frac{\omega}{2NkT}\text{Tr}_s[\{\langle\tilde{\mathcal{M}}_x(\Omega,i\omega)\rangle + \langle\tilde{\mathcal{M}}_x(\Omega,-i\omega)\rangle\}\mathcal{M}_x] \quad (B1)$$

where $\mathcal{M}_x$ is the x component of the magnetization operator and $\tilde{\mathcal{M}}_x(i\omega)$ is the Laplace transform of $\mathcal{M}_x(t)$, the magnetization operator in the Heisenberg representation given by

$$\mathcal{M}_x(t) \equiv e^{(i\mathcal{H}^x - \Gamma_\Omega)t}\mathcal{M}_x \quad (B2a)$$

so

$$(i\omega - i\mathcal{H}^x + \Gamma_\Omega)\tilde{\mathcal{M}}_x(\Omega,i\omega) = \mathcal{M}_x \quad (B2b)$$

Also

$$\tilde{\mathcal{M}} = \beta_e\bar{g}\cdot\mathbf{S}/\hbar \quad (B3)$$

The angular brackets in eq B1 imply ensemble averaging over the stochastic variables Ω, while the trace represented by Tr_s is over all spin states. Other definitions are as previously given.[24,25]

We now consider the case of $S = 1/2$, and we recognize that $\mathcal{M}_x = \mathcal{M}_x^\dagger$ while $\tilde{\mathcal{M}}_x(\Omega,i\omega) = \tilde{\mathcal{M}}_x(\Omega,-i\omega)^\dagger$, so

$$\langle+|\tilde{\mathcal{M}}_x(\Omega,i\omega)|-\rangle = \langle-|\tilde{\mathcal{M}}_x(\Omega,-i\omega)|+\rangle^* \quad (B4)$$

Also

$$\mathcal{M}_{\pm1} = \mp(1/(2)^{1/2})[\mathcal{M}_x \pm i\mathcal{M}_y] \quad (B5a)$$

$$\mathcal{M}_0 = \mathcal{M}_z \quad (B5b)$$

in terms of the raising and lowering operators (in irreducible tensor form) with equivalent expressions for $S_{\pm1}$ and S_0. We now introduce the irreducible tensor components of **g**: [i.e., $\bar{g} \equiv \frac{1}{3}(g_{xx} + g_{yy} + g_{zz})$, $g_0 \equiv (3/(16)^{1/2})(g_{zz} - \bar{g})$, $g_{\pm1} = \mp g_{zx} - ig_{zy}$, $g_{\pm2} = \frac{1}{2}(g_{xx} - g_{yy} \pm 2ig_{xy})$]. Then eq B3 may be rewritten for $\mathcal{M}_{\pm1}$ as

$$\mathcal{M}_{\pm1} = \hbar^{-1}\beta_e\left(\bar{g}S_{\pm1} - \frac{g_0}{(6)^{1/2}}S_{\pm1} - g_{\pm2}S_{\mp1} + \frac{1}{(2)^{1/2}}g_{\pm1}S_0\right) \quad (B6)$$

where all irreducible tensor components are expressed in the lab frame. The first term on the right of eq B6 is the usual term for an isotropic g value, while the other three terms represent corrections for anisotropy in the **g** tensor. We then have for $\mathcal{M}_x$

$$\mathcal{M}_x = \frac{\beta_e}{(2\hbar)^{1/2}}\left[\left(\bar{g} - \frac{g_0}{(6)^{1/2}}\right) \times \right.$$
$$\left. (S_{-1} - S_{+1}) + (g_{+2}S_{-1} - g_{-2}S_{+1}) + (g_{+1} - g_{-1})S_0/(2)^{1/2}\right] \quad (B7)$$

which yields

$$\langle\pm|\mathcal{M}_x|\mp\rangle = \frac{\beta_e}{2\hbar}\left[\bar{g} - \frac{g_0}{(6)^{1/2}} + g_{\mp2}\right]\langle\pm|S_\pm|\mp\rangle \quad (B8a)$$

$$\langle\pm|\mathcal{M}_x|\pm\rangle = \frac{\beta_e}{2\hbar}[g_{-1} - g_{+1}]\langle\pm|S_z|\pm\rangle \quad (B8b)$$

(where $S_\pm = \mp(2)^{1/2}S_{\pm1}$), as the matrix elements of $\mathcal{M}_x$. Therefore eq B1 becomes (cf. eq B4)

$$\chi''_{xx}(\omega) \propto$$
$$2\,\text{Re}\{[\langle-|\mathcal{M}_x(\Omega,i\omega)|+\rangle + \langle-|\mathcal{M}_x(\Omega,-i\omega)|+\rangle]\langle+|\mathcal{M}_x|-\rangle +$$
$$\langle+|\mathcal{M}_x(\Omega,i\omega)|+\rangle\langle+|\mathcal{M}_x|+\rangle + \langle-|\mathcal{M}_x(\Omega,i\omega)|-\rangle\langle-|\mathcal{M}_x|-\rangle\} \quad (B9)$$

We must now transform the irreducible tensor components g_M from the lab frame to the molecular frame (given by $\hat{g}_K$) according to[3,8]

$$g_M = \sum_K \mathcal{D}_{MK}^2(-\Omega)\hat{g}_K = \sum_K(-)^{K-M}\mathcal{D}_{-K,-M}^2(\Omega)\hat{g}_K \quad (B10)$$

where Ω now represents the Euler angles for the transformation. Equations B8, B9, and B10 with eq B2b now determine the complete solution. We can now expand $\mathcal{M}_x(\Omega,i\omega)$ in the complete set of eigenfunctions, $G_{KM}^L(\Omega) = [(2L+1)/(8\pi^2)]^{1/2}\mathcal{D}_{KM}^L(\Omega)$,[3,6,8] where, for axially symmetric problems, we may let $K = 0$ in eq B10.

The overall slow-tumbling solution may be written in matrix format as[3,22]

$$\chi''_{xx}(\omega,B) = \frac{\omega}{NkT}\text{Im }\mathbf{U}^{Tr}\cdot\mathbf{C} \quad (B11a)$$

where

$$\mathbf{C} = \mathbf{A}^{-1}\cdot\mathbf{U} \quad (B11b)$$

$$\mathbf{A} \equiv [i\mathbf{L} - i\omega\mathbf{1} - \mathbf{\Pi}] \quad (B11c)$$

where $\mathbf{\Pi}$ is the "diffusion matrix", $\mathbf{L}$, the "spin matrix", $\mathbf{C}$ is a vector of the coefficients (cf. eq 2a),[26] and $\mathbf{U}$ is a vector of transition moments. In particular for the present case, $U_{KM}^L(i)$ the L,K,Mth term for the ith (allowed) transition between states a and a' is given by

$$U_{KM}^L(i) = \int P_0^{1/2}(\Omega)G_{KM}^{*L}(\Omega)\langle a|\mathcal{M}_x|a'\rangle\,d\Omega \quad (B12)$$

and is affected by the anisotropic contributions in eq B8, while $\mathbf{\Pi}$, $\mathbf{L}$ (hence $\mathbf{A}$), and $\mathbf{C}$ are not otherwise directly modified from what has already been given in the main body of the text by the anisotropy in the transition moment. For an isotropic fluid $P_0(\Omega) = 1/(8\pi^2)$ and $\mathbf{U}^{Tr}$ is then simply the transposed complex-conjugate vector of $\mathbf{U}$ (for anisotropic fluids see ref 4).

Thus, for isotropic fluids and an axially symmetric **g** tensor eq B12 becomes

$$U_{KM}^L(i) = \frac{\beta_e}{2\hbar}\left[\left(\bar{g}\delta_{L,0}\delta_{M,0} - (\hat{g}_0/(30)^{1/2})\delta_{L,2}\delta_{M,0} + \frac{\hat{g}_0}{(5)^{1/2}}\delta_{L,2}\delta_{M,-2}\right)\right]\delta_{K,0}\langle-|S_-|+\rangle \quad \text{(B13a)}$$

where for the ith transition: $a \to a'$, $\langle a|S_-|a'\rangle = \langle-|S_-|+\rangle$, and

$$U_{KM}^L(\pm) = \frac{\beta_e\hat{g}_0}{2(5\hbar)^{1/2}}(\delta_{M,1} - \delta_{M,-1})\delta_{L,2}\delta_{K,0}\langle\pm|S_z|\pm\rangle \quad \text{(B13b)}$$

where $\langle a|S_z|a\rangle = \langle-|S_z|-\rangle$ and $\langle a'|S_z|a'\rangle = \langle+|S_z|+\rangle$.

We now introduce the approximation, valid for vanadyl, of relatively small g anisotropy, i.e., $\bar{g} \gg |\hat{g}_0|$, so the corrections to the U_{KM}^L are small. This is also actually necessary for the high-field approximation utilized in section II. Given that high-field approximation as well as the additional high-field requirement $|B_0| \gg |B_1|$, so the counterrotating and diagonal components of eq B9 may be neglected when near the normal ESR resonance, then it is also just sufficient to let $U_{KM}^L(\pm) \approx 0$ since eq B13b is associated with near-zero (off-resonant) frequencies. We note that the term $(\hat{g}_0/(5)^{1/2})\delta_{L,2}\delta_{M,-2}$ in eq B13a will only very weakly introduce a new set of coefficients C_{KM}^L with $M = \pm 2$ (i.e., of order $^1/_5(\hat{g}_0/\bar{g})^2$), and correction due to the term $(\hat{g}_0/(30)^{1/2})\delta_{L,2}\delta_{M,0}$ is an easy one to introduce into the solution (eq B11) but also of order $^1/_{30}(\hat{g}_0/\bar{g})^2$ in importance.

We found, by direct simulation of the rigid-limit vanadyl spectra, that effects from an orientation-dependent transition moment were small enough to be unimportant in the rigid limit, so we did not include the correction terms for the slow-motional simulations.

(2) Field- vs. Frequency-Swept ESR Spectra. In order to obtain $\chi''(\omega,B_0)$ given by eq B11a, one must diagonalize the **A** matrix. For the case of frequency-swept, fixed-field spectra, the computation of $\chi''(\omega,B_0)$ requires only a single diagonalization since the frequency ω lies only on the diagonal of the **A** matrix. However, for computation of $\chi''(\omega,B_0)$ for field-swept, fixed-frequency spectra, the problem could become much more laborious, since the field variable, B_0, appears in off-diagonal elements of **A** (cf. eq 1). As a consequence, **A** must, in principle, be diagonalized for each field value over the sweep width of the spectrum.

Even though ESR spectra are obtained by field-swept, fixed-frequency experiments, one may generally construct $\chi''(\omega,B_0)$ to a good approximation by a single diagonalization in which $\mathcal{H}_1(\Omega)$ is based on the value of B_0 at the center of the spectrum, and $(\omega - \omega_0)$ which appears along the diagonal of **A** is the swept variable. This has been demonstrated for the case of nitroxide free radical spectra.[3,6] In the case of nitroxides, the entire sweep width is ~40 G and centered around 3300 G. Thus, the error in choosing the dc field value within this sweep width is <1%. However, for vanadyl spectra the sweep width is ~1500 G and centers around 3600 G. Thus, the error in computing vanadyl ESR spectra as though they were frequency-swept spectra could be as great as 20%. The effect of changing the value of the dc field in a frequency-swept computation is shown in Figure 10A. As one can see, in the case of this slow-motional spectrum, there is a slight but noticeable difference in both the intensities and positions of the resonance lines for a 10% change in B_0.

In order to test the validity of computing vanadyl spectra as though they were frequency-swept spectra, we
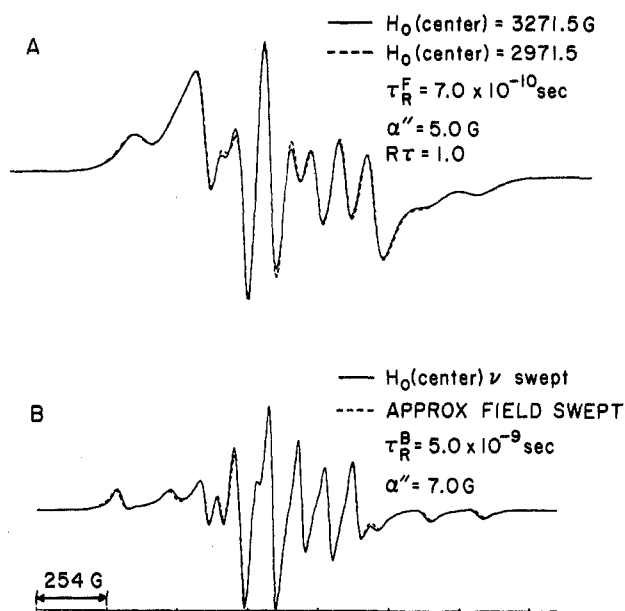
Figure 10. Comparison of frequency-swept vs. field-swept spectral simulations in the slow-motional region.

developed an "approximate" field-swept computation of $\chi''(\omega,B_0)$. Here, the spectrum is divided into n (≈ 6) equal field intervals, and $\chi''(\omega,B_0)$ is formed by summing the spectra computed for each interval (with $B_0^{(n)}$ being taken at the center of each respective interval). Comparison of vanadyl rapid-motional spectra computed by this approach with full-field-swept computations gave exact agreement and provided confidence in this approach. In Figure 9B we compare a slow-motional frequency-swept spectrum with that computed by the approximate-field-swept technique. As one can see, only very slight discrepancies occur. As the rigid limit is approached, however, one may expect somewhat greater discrepancies between frequency-swept and field-swept spectra as the derivative lines become narrower.

(3) Effect of van Vleck Transformation on the U Vector. We consider the effect of a van Vleck transformation which block diagonalizes the **A** matrix of eq B11c on the complete solution, eq B11a. If we consider the approximate decoupling of the "eigenstate-pair" coefficients in the high-field approximation as given in section II, then eq B11a becomes

$$\chi''_{xx} \propto \left[U_1^{Tr}, 0\right]\left[1 + \begin{pmatrix} 0 & S_{12} \\ S_{21} & 0 \end{pmatrix}\right]\begin{bmatrix} A'_1{}^{-1} & 0 \\ 0 & A'_2{}^{-1} \end{bmatrix} \times \left[1 - \begin{pmatrix} 0 & S_{12} \\ S_{21} & 0 \end{pmatrix}\right]\begin{bmatrix} U_1 \\ 0 \end{bmatrix} \quad \text{(B14)}$$

where A'_1 and A'_2 are the block diagonalized **A** matrix, where $\mathbf{A} = (\mathbf{A}_{11}\ \mathbf{A}_{12})$, and $\mathbf{S}_{ij}$ are the van Vleck transformation matrices, and are of order $|\mathcal{H}_1^{nonsec}(\Omega)/\omega_0| \ll 1$. Upon multiplying out eq B14 one obtains

$$\chi''_{xx} \propto U_1^{Tr}A'_1{}^{-1}U_1 - U_1^{Tr}S_{12}A'_2{}^{-1}S_{21}U_1 \quad \text{(B15)}$$

The analysis of section II is based upon the first term of eq B15 involving $A'_1 = A_{11}$ + nonsecular corrections, as given in section II. The additional term in eq B15 was not included in section 2; it is of the order $|\mathcal{H}_1^{nonsec}(\Omega)/\omega_0|^2$ smaller than the dominant term, i.e., one order higher than the terms being retained. Also A'_2 will consist of coefficients C_{KM}^L which are resonant for $\omega \approx 0$, so they are way off resonance and therefore negligible when $\omega \approx \omega_0$ in the high-field approximation.

A similar argument to the above can be given to justify the approximation of eq 6a in Appendix A; i.e., one writes

A'_1 in terms of the sum and difference coefficients (cf. eq 6a). Then an analysis of eq B14 shows that the effects of the neglected coefficients are of the order $(\epsilon/X)^2$ where ϵ's, the nonsecular corrections of eq 6, are of the order $|\mathcal{H}_1^{nonsec}(\Omega)|^2/\omega_0$ and X, the regular secular and pseudosecular contributions in eq 2a, are of the order $|\mathcal{H}_1(\Omega)^{sec+pseudosec}|$. So $(\epsilon/X)^2$ is of the order $(\mathcal{H}_1(\Omega)/\omega_0)^2$ and again is one order higher than terms being retained. [The argument about "nonresonant" coefficients does not apply here.]

Appendix C. The SLE and Motionally Narrowed Line Widths

It is well-known that the first derivative Lorentzian line widths (in gauss) of motionally narrowed spectra may be expressed as[27]

$$\Delta H(M,\tau_R) = \alpha + \beta M + \gamma M^2 + \delta M^3 \qquad (C1)$$

where M is the nuclear spin quantum number of the Lorentzian resonance line under consideration, and τ_R is the rotational correlation time.

The coefficients of M may be obtained via the stochastic Liouville method by considering only the $L = 0$ and $L = 2$ terms of eq 2a and 6. By applying perturbation theory to the resulting simplified relaxation matrix and taking the imaginary part (i.e., the line width part) of the resulting expressions, one obtains upon grouping terms with respect to their power of M

$$\alpha = \alpha'' + \frac{2\tau_R}{(3)^{1/2}|\gamma_e|}\left\{\frac{F^2}{5}\left[1 + \frac{3}{4}\mu + \frac{3}{28}\frac{F}{\hat{\omega}_0}\right] + \right.$$
$$\left. \frac{I(I+1)}{5}\left[D^2 + \frac{7}{3}D^2\mu - \frac{5D^2F}{42\hat{\omega}_0} + \frac{1}{4}\left(\frac{2}{3}\right)^{1/2}\frac{FDA_0}{\hat{\omega}_0}\right]\right\} \qquad (C2a)$$

$$\beta = \frac{2\tau_R}{(3)^{1/2}|\gamma_e|}\left\{-\frac{4}{5}\left(\frac{2}{3}\right)^{1/2}FD\left[1 + \frac{3}{4}\mu + \frac{9}{56}\frac{F}{\hat{\omega}_0}\right] - \right.$$
$$\frac{I(I+1)}{15}\frac{D^2A_0}{\hat{\omega}_0} + $$
$$\left. \frac{1}{21}\left(\frac{2}{3}\right)^{1/2}[I(I+1)]\frac{D^3}{\hat{\omega}_0} - \frac{aD^2}{10\hat{\omega}_0} + \frac{1}{14}\left(\frac{2}{3}\right)^{1/2}\frac{D^3}{\hat{\omega}_0}\right\} \qquad (C2b)$$

$$\gamma = $$
$$\frac{2\tau_R}{(3)^{1/2}|\gamma_e|}\left\{\frac{8}{15}D^2\left[\frac{5}{8} - \frac{\mu}{8} + \frac{41}{112}\frac{F}{\hat{\omega}_0}\right] - \frac{1}{20}\left(\frac{2}{3}\right)^{1/2}\frac{FDA_0}{\hat{\omega}0}\right\} \qquad (C2c)$$

$$\delta = \frac{2\tau_R}{(3)^{1/2}|\gamma_e|}\left\{\frac{1}{15}\frac{A_0D^2}{\hat{\omega}_0} - \frac{17}{105}\left(\frac{2}{3}\right)^{1/2}\frac{D^3}{\hat{\omega}_0}\right\} \qquad (C2d)$$

where

$$\hat{\omega}^{-1} \equiv \left[\frac{1}{\omega_0} + \frac{1}{\omega_x}\right]$$

$$\omega_x^{-1} \equiv \frac{\omega_0\tau_R^2}{1 + \omega_0^2\tau_R^2}$$

$$\mu = \frac{1}{1 + \omega_0^2\tau_R^2}$$
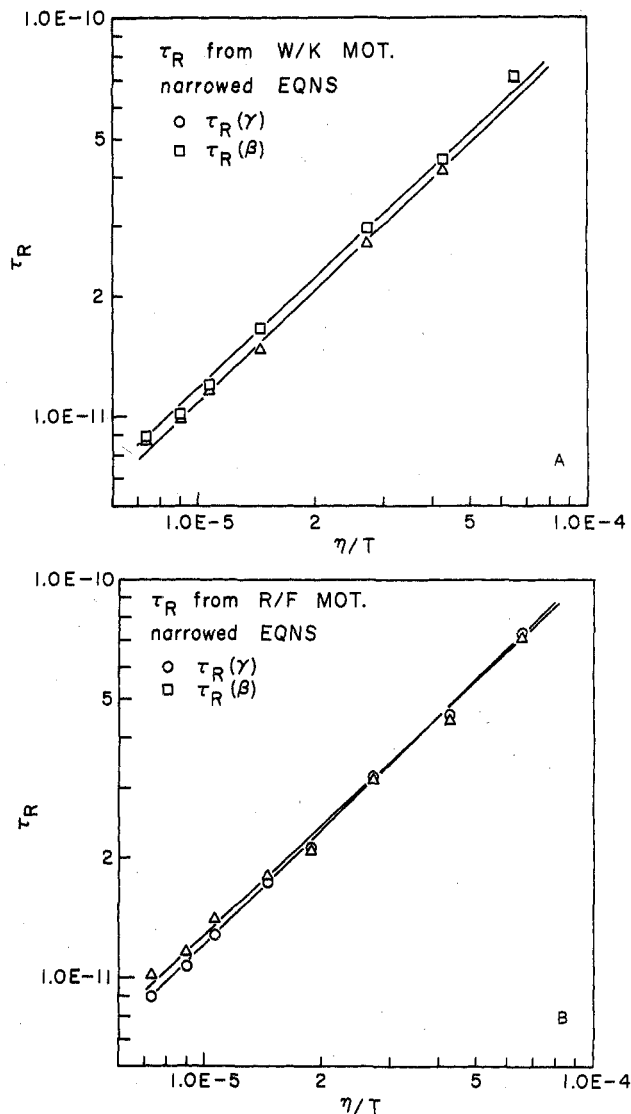
Figure 11. τ_R vs. η/T from motionally narrowed expressions of (A) Wilson and Kivelson and (B) stochastic Liouville result, eq C2: (O) $\tau_R(\gamma)$; ($\triangle$) $\tau_R(\beta)$.

where α'' is the residual line-width component (in gauss) that corresponds to T_2^{-1} in eq 2a, and τ_R is the rotational correlation time and corresponds to τ_2 in eq 2a. [In the motionally narrowed region all reorientational models yield the same line width for a given value of τ_R.][6,22]

Equations C1 and C2 relate τ_R to the measured line widths and the experimentally determined $g_{\parallel}, g_{\perp}, A_{\parallel}$, and $A_{\perp}$ values. In practice τ_R is obtained from β and γ because of the uncertainty in α and the experimental error in determining δ.

Equations C1 and C2 agree in essence with the linewidth formulae of Wilson and Kivelson that were obtained from motionally narrowed theory. Slight discrepancies occur because of differences in the perturbation treatment of the nonsecular terms rather than any fundamental differences between motionally narrowed theory and the stochastic Liouville method. These formulae were applied to $VO(acac)_2$ line-width data published in ref 16, and $\tau_R(\beta)$ and $\tau_R(\gamma)$ vs. η/T are shown in Figure 11. As can be seen, $\tau_R(\gamma)$ is consistently a little larger than $\tau_R(\beta)$ via the usual motionally narrowed formulae,[16,27] while via eq C2 this difference is generally reduced. There is no theoretical reason why $\tau_R(\beta)$ and $\tau_R(\gamma)$ should be different, so one might favor eq C2. In comparing parts A and B of Figure 11, one sees that the slope of τ_R vs. η/T of Figure 11 is

greater than that of Figure 10. Thus, in general, for a given η/T, τ_R computed via eq C2 will be slightly larger than that computed via the Wilson–Kivelson equations.

Lastly, we note that there is no indication in these results on VO(acac)$_2$ in toluene of any substantial departure of the spectral densities from Debye-type spectral densities (i.e., the definitions of μ and ω_x in eq C2 such as was found for PD-Tempone in toluene.[12] This is, perhaps, consistent with the slow-motional result that ESR spectra of the vanadyl complexes are fit by Brownian diffusion while PD-Tempone is fit by jump diffusion.

References and Notes

(1) R. F. Campbell and M. W. Hanna, *J. Phys. Chem.*, **80**, 1892 (1976), and references therein.
(2) G. V. Bruno, J. K. Harrington, and M. P. Eastman, *J. Phys. Chem.*, **81**, 1111 (1977).
(3) J. H. Freed, G. V. Bruno, and C. F. Polnaszek, *J. Phys. Chem.*, **75**, 3385 (1971).
(4) C. F. Polnaszek, G. V. Bruno, and J. H. Freed, *J. Chem. Phys.*, **58**, 3185 (1973).
(5) G. V. Bruno, J. K. Harrington, and M. P. Eastman [*J. Phys. Chem.*, **82**, 2582 (1978)] more recently considered VO^{2+} in nematic solvents. There they observe non-Brownian effects in the nematic phase analogous to those seen by Polnaszek and Freed [*J. Phys. Chem.*, **79**, 2283 (1975)] for nitroxide probes, which are also interpreted in terms of nematic phase slowly relaxing structural effects. These, however, occur mainly in the incipient slow-tumbling region where the non-Brownian models, which would be important in isotropic (or ordered) fluids, have little spectral effect, and for which the nonsecular analysis of Bruno et al. is more successful. They do, however, improve on their nonsecular analysis somewhat by the inclusion of effects on forbidden transitions in this newer work but otherwise retain the same approximate form.
(6) S. A. Goldman, G. V. Bruno, C. F. Polnaszek, and J. H. Freed, *J. Chem. Phys.*, **54**, 716 (1972).
(7) This approximation is commonly made for nitroxides[3,4] for which the nuclear Zeeman term is more important, and it results in greatly reducing the number of coefficient equations to be solved.
(8) A. R. Edmonds, "Angular Momentum in Quantum Mechanics", Princeton University Press, Princeton, NJ, 1957.
(9) S. A. Goldman, G. V. Bruno, and J. H. Freed, *J. Chem. Phys.*, **58**, 3185 (1973).
(10) G. V. Bruno, Ph.D. Thesis, Cornell University, Ithaca, NY, 1973.
(11) We thank Professor N. D. Chasteen for a copy of his rigid-limit program.
(12) J. S. Hwang, R. P. Mason, L. P. Hwang, and J. H. Freed, *J. Phys. Chem.*, **79**, 489 (1975).
(13) Actually, in Figure 6 one may note some deviation from the linear dependence for the most viscous case. While a more detailed study would be required to see if this were significant, an interesting possibility could be the following. A useful expression for τ_L^{-1} for jump diffusion is $\tau_L^{-1} = L(L + 1)R/[1 + L(L + 1)R\tau]$ where R is the rotational diffusion coefficient and τ is the mean jump time.[6] Now as $R\tau \rightarrow 0$ simple Brownian motion is recovered. However, if $R\tau$ is small (e.g., 0.1) but not zero, then, in the faster motional regions where the spectrum is determined by small values of L, τ_L^{-1} is well approximated by Brownian motion. However, for slower motions (which in fact may be too slow to show any model dependence directly in the "near-rigid" spectrum) where larger L values become important (e.g., $L \gg 4$) the corresponding τ_L^{-1} become more non-Brownian. This last point in Figure 6 is in the direction anticipated for a small jump-type correction (cf. Figure 9 and ref 6 and 12).
(14) D. Hoel and D. Kivelson, *J. Chem. Phys.*, **62**, 4535 (1975).
(15) C. F. Polnaszek and J. H. Freed, *J. Phys. Chem.*, **79**, 2283 (1975).
(16) R. Wilson and D. Kivelson, *J. Chem. Phys.*, **44**, 154 (1966).
(17) NBS Circular, Suppl. 440 (1958).
(18) L. J. Boucher, E. C. Tynan, and T. F. Yen, *Inorg. Chem.*, **7**, 731 (1968).
(19) P. J. McCarthy, R. J. Hovey, K. Ueno, and A. E. Martell, *J. Am. Chem. Soc.*, **77**, 5820 (1955). The product was recrystallized from water three times.
(20) A. C. Hazell, *J. Chem. Soc. London*, 5745 (1963).
(21) A. J. Barrow, J. Lamb, and A. J. Matheson, *Proc. R. Soc. London, Ser. A*, **292**, 322 (1966); "International Critical Tables", Vol. 1, 1930, p 211.
(22) J. H. Freed in "Spin Labeling, Theory and Applications", L. J. Berliner, Ed., Academic Press, New York, 1976, Chapter 3.
(23) Note that for all but the motionally narrowed to incipient slow-motional regions a minimum of one megabyte of core is required.
(24) J. H. Freed, G. V. Bruno, and C. F. Polnaszek, *J. Chem. Phys.*, **55**, 5270 (1971).
(25) J. H. Freed in "Electron-Spin Relaxation in Liquids", L. T. Muus and P. W. Atkins, Ed., Plenum Press, New York, 1972, Chapter 14.
(26) The analysis based upon eq B1 more naturally leads to a somewhat different set of coefficients $a_{KM}^\prime$ which, however, are readily related to the coefficients $C_{KM}^\prime$ used in section II, as discussed in ref 24.
(27) D. Kivelson, *J. Chem. Phys.*, **33**, 1094 (1960); J. H. Freed and G. K. Fraenkel, *Ibid.*, **39**, 326 (1963).

Comparative Rates of Exchange behind Reflected Shock Waves. 2. ¹⁵NO + C¹⁸O vs. ¹⁵NO + N₂[1]

A. F. Bopp, R. D. Kern,* T. Niki, and G. M. Stack

Department of Chemistry, University of New Orleans, New Orleans, Louisiana 70122 (Received: February 11, 1980)

The rates of isotopic exchange of nitric oxide with nitrogen and carbon monoxide were studied over the temperature range 2700–3800 K by analyzing the gas from the reflected shock zone at 20-μs intervals with a time-of-flight mass spectrometer. Two mixtures containing 4% ¹⁵NO–4% N₂ in one and 4% ¹⁵NO–4% C¹⁸O in the other were each diluted with a mixture of inert gases (Ne–Ar–Kr). The reacting gases were sampled dynamically in order to determine the time dependence of the products; i.e., m/e 29 and 30 for the first mixture and m/e 28 and 33 for the second mixture. The exchange of nitric oxide and carbon monoxide took place readily over the range investigated. The reaction profiles displayed nonlinear growth of the products with respect to reaction time. Computer simulation of the product profiles assuming an atomic mechanism revealed reasonable agreement with the experimental data. In contrast to ¹⁵NO + C¹⁸O, the exchange of ¹⁵NO + N₂ did not occur to any measurable extent in accordance with the predictions of an atomic mechanism.

Introduction

In a recent report from this laboratory[2] the rate of exchange of C¹⁸O with CO₂ was compared to the exchange rate of ¹³CO with CO₂. It was observed that the rate of the former exceeded that of the latter and that an atomic mechanism was insufficient to account for the amount of product conversion in either of the two exchanges, particularly at the lower-temperature end of the study. It was proposed that molecular transition state channels were being utilized.